Polymer maximum drag reduction: A unique transitional state

By Y. Dubief†, C. M. White‡, E. S. G. Shaqfeh AND V. E. Terrapon

1. Motivation and objectives

In spite of the many significant advances in the understanding of polymer drag reduction, at least two fundamental questions remain open:(a) What is the maximum drag reduction (MDR) state? and (b) How does one predict the magnitude of drag reduction from the properties of the flow and polymer solution? The present study answers the first question with the identification of MDR as a unique transitional state, which is a necessary step in the process of addressing the second question.

Virk *et al.* (1970) empirically defined the log region of the velocity profile of MDR as,

$$U^+ = 11.7\log(y^+) - 17 \tag{1.1}$$

from experimental data. The superscript $^+$ denotes the normalization of velocity and length by u_τ and ν/u_τ, respectively, where u_τ is the skin friction velocity of the flow and ν is the fluid viscosity. Among the many experiments that studied MDR, Warholic *et al.* (1999) measured velocity profiles in close agreement with Eq. (1.1) throughout the log region of a channel flow with homogenous polymer concentration. In experiments where polymers are injected at the wall of boundary layer flows, White *et al.* (2004) and Somandepalli *et al.* (2010) obtained velocity profiles that follow Eq. (1.1) up to $y^+ \simeq 50 - 100$. The outer region shows a log behavior, yet with a slightly smaller slope than Eq. (1.1). Similar observations were made in the DNS of drag reduction in turbulent boundary layers by Dimitropoulos *et al.* (2005, 2006). In these experiments or simulations, arguments may be made that the departure from the MDR asymptotic velocity profile is the likely result of specific boundary conditions of the flow or polymer concentrations.

DNS efforts in channel flows achieved MDR only for transient durations in large computational domain, as demonstrated by Min *et al.* (2003), or steadily in a minimal flow unit (Jimenéz & Moin 1991) computational domain (Ptasinski *et al.* 2003; Dubief *et al.* 2005). Most simulations predicted a regime approaching MDR. High drag reduction (HDR) is characterized by an increase in the slope of the log-law, by opposition to LDR (low drag reduction), observed for $DR \lesssim 40\%$, where the log law is only shifted upward (Warholic *et al.* 1999; Min *et al.* 2003; Dubief *et al.* 2004). Hereafter DR denotes the drag reduction of a polymeric flow, which is the percentage decrease of pressure gradient relative to the pressure gradient for the Newtonian flow in a channel flow driven by constant mass flow.

Regardless of the peculiarities of every experiment or simulation that achieved or closely approached MDR, it is undeniable that Virk's empirical log law, Eq. (1.1), is universally satisfied at least in the inner region of the flow. Now, to formulate our hypothesis, we turn to the mechanism of polymer drag reduction. Dubief *et al.* (2004) showed that polymer work, or elastic energy, opposes the upwash and downwash flows generated by

† School of Engineering and Vermont Advanced Computing Center, University of Vermont
‡ Mechanical Engineering Department and Center for Fluid Physics, University of New Hampshire

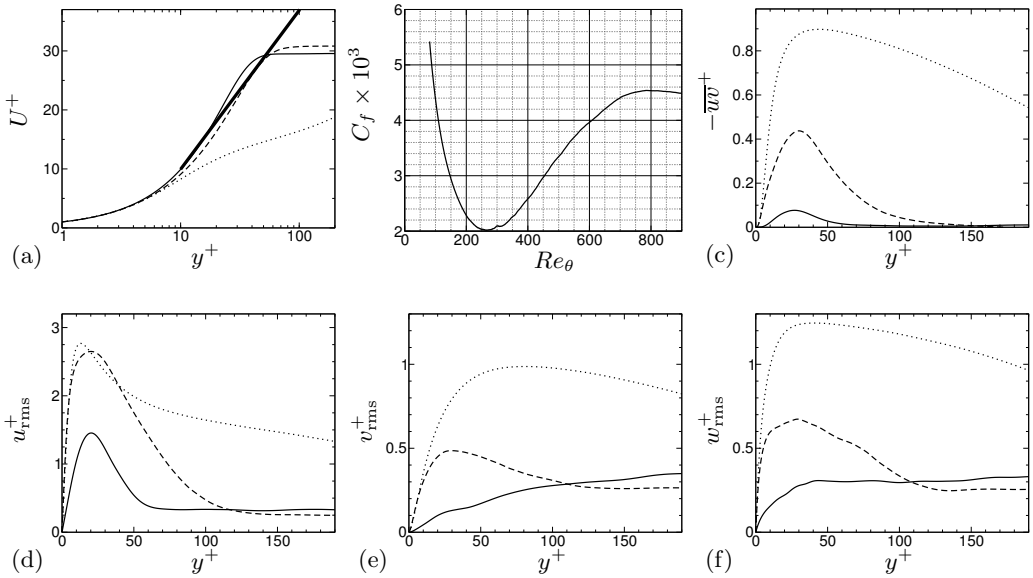

FIGURE 1. Velocity statistics of the transitional boundary layer simulation of Wu & Moin (2009) for two states whose velocity profiles approach closely Virk's asymptotic velocity profile (Eq. 1.1). (a) Shows Eq. (1.1) ▬▬, $Re_\theta = 200$ ——, $Re_\theta = 300$ – – –, and $Re_\theta = 900$ ····· (fully turbulent flow). (b) Plots the distribution of the skin friction coefficient C_f as a function of the Reynolds number based on the local momentum thickness θ. (c, d, e and f) Compare Reynolds shear stress, RMS of streamwise, wall-normal and spanwise velocity fluctuations, respectively, for the three flow states as shown in (a).

quasi-streamwise vortices. Kim *et al.* (2007) demonstrated the same effect in the form of negative torque applied by polymers to vortices. Dubief *et al.* (2004) also captured a coherent transfer of elastic energy into turbulent kinetic energy in high-speed streaks, and speculated that this turbulence-enhancing phenomenon may play a role in MDR. A consequence of the weakening of near-wall vortices is the increase in coherence of high- and low-speed streaks, as observed for instance by White *et al.* (2004). The extrapolation of the mechanism of polymer drag reduction to its maximum efficiency should therefore lead to a turbulent state devoid of vortices and driven by highly organized streaks, a state commonly observed in early stages of transition to turbulence in wall-bounded flows.

Our hypothesis is therefore that MDR corresponds to a transitional state whose growth is inhibited by the action of elastic energy onto emerging vortices. To test our hypothesis, we first identify the region of the transitional boundary layer simulation of Wu & Moin (2009) where the mean velocity profile best approaches Eq. (1.1). Once this specific state is identified, the assumption is validated using DNS of polymeric channel flows that achieve MDR. In particular, a simulation of the transition to turbulence demonstrates the growth inhibition of the specific transitional state. Remarkably, MDR is also attained from fully turbulent initial conditions. Another significant contribution of this brief is the discovery of purely elastic instabilities which play a major role in the transition to turbulence of polymeric flows and on the fluctuations of the MDR regime.

2. Identification of a MDR-like transitional state

Using the statistical database of the transitional boundary layer simulation of Wu & Moin (2009), we compare the evolution of mean velocity profiles in the transitional region to Eq. (1.1). Fig. 1a establishes that the region between $Re_\theta = 200$ and 300 best approaches Virk's asymptotic velocity profile. Here the Reynolds number, Re_θ, is based on the momentum boundary layer thickness θ. The evolution of the skin-friction coefficient as a function of Re_θ in Fig. 1b , indicates that the region $200 \leq Re_\theta \leq 300$ corresponds to the minimum of C_f, caused by the breakdown of the linear instabilities. In this region, vortices emerge and turbulent spots form; the Reynolds shear stress consequently increases from almost negligible levels at $Re_\theta = 200$ to roughly half its level in fully turbulent flows at Re_θ (Fig. 1c). Fig. 1d shows a twofold increase of the streamwise velocity fluctuations between $Re_\theta = 200$ and 300, for which the maximum is slightly higher that the maximum of $u^+_{\rm rms}$ in fully developed turbulence. Figs. 1e-1f highlight the emergence of vortices with a significant increase in wall-normal and spanwise velocity fluctuations and, for both velocity components, vertical profiles that are qualitatively identical to fully developed turbulence. The lower intensity of turbulence in the transverse direction is caused by the intermittence of vortices and turbulent spots in this region of the transitional flow.

3. Direct numerical simulations of MDR

3.1. *Methods*

The numerical method is described in Dubief *et al.* (2005) and briefly reviewed here. Channel flow simulations are performed in a cartesian domain defined by the orthonormal vector base $(\mathbf{e}_x, \mathbf{e}_y, \mathbf{e}_z)$ where x, y and z are the streamwise, wall-normal and spanwise directions, respectively. The components of the velocity vector $\mathbf{u}$ are u, v, and w. For a viscoelastic flow, the governing equations for conservation of mass and transport of momentum are:

$$\boldsymbol{\nabla} \cdot \mathbf{u} = 0 \text{ and} \tag{3.1}$$

$$\frac{\partial \mathbf{u}}{\partial t} + (\mathbf{u} \cdot \boldsymbol{\nabla})\mathbf{u} = -\boldsymbol{\nabla} p + \frac{\beta}{Re}\nabla^2 \mathbf{u} + \frac{1-\beta}{Re}\boldsymbol{\nabla} \cdot \mathbf{T} + g(t)\mathbf{e}_x \tag{3.2}$$

where $g(t) = -(dP/dx)$ is used to maintain constant mass flux. The parameter β is the ratio of solvent viscosity to the zero-shear viscosity of the polymer solution and affects both the viscous stress and polymer stress terms in Eq. (3.2). The polymer stress tensor $\mathbf{T}$ is computed using the FENE-P (Finite Elastic Non-linear Extensibility-Peterlin) model (Bird *et al.* 1987):

$$\mathbf{T} = \frac{1}{We}\left(\frac{\mathbf{C}}{1 - \mathrm{tr}(\mathbf{C})/L^2} - \mathbf{I}\right) , \tag{3.3}$$

where the tensor $\mathbf{C}$ is the local conformation tensor of the polymer solution and $\mathbf{I}$ is the unit tensor. The properties of the polymer solution are β, the relaxation time λ, here based on the convection scales ($We = \lambda U_c/H$) and the maximum polymer extension L. The FENE-P model assumes that polymers may be represented by a pair of beads connected by a non-linear spring and defined by the end-to-end vector $\mathbf{q}$. The conformation tensor is the phase-average of the tensorial product of the end-to-end vector $\mathbf{q}$ with itself, $\mathbf{C} = \langle \mathbf{q} \otimes \mathbf{q} \rangle$ whose transport equation is

$$\frac{\partial \mathbf{C}}{\partial t} + (\mathbf{u} \cdot \boldsymbol{\nabla})\mathbf{C} = \mathbf{C}(\boldsymbol{\nabla}\,\mathbf{u}) + (\boldsymbol{\nabla}\,\mathbf{u})^{\mathrm{T}}\mathbf{C} - \mathbf{T} \, . \tag{3.4}$$

On the left hand side of Eq. (3.4), the first two terms are responsible for the stretching of polymers by hydrodynamic forces, whereas the third term models the internal energy that tends to bring stretch polymers to their least energetic state (coiled). The FENE-P model has demonstrated its ability to capture the physics of polymer drag reduction (*e.g.* Sureshkumar *et al.* 1997; De Angelis *et al.* 2002; Ptasinski *et al.* 2003; Min *et al.* 2003; Dubief *et al.* 2004). Eqs. (3.2-3.4) are solved using finite differences on a staggered grid (see Dubief *et al.* 2005, for details). Time advancement is carried out using a third-order explicit Runge-Kutta for non linear terms and second-order implicit Crank-Nicolson for diffusive terms. The CFL, fixed at 1.0 for Newtonian flows, has to be lowered to 0.2 for viscoelastic flows with large We and L and even 0.1 during the introduction of polymers in a turbulent flow.

3.2. *Initial conditions*

A non-trivial issue in the simulation of transition in periodic channel flows is the initial condition of the polymer field. In previous studies carried out by the present authors, polymers in isotropic configuration ($\mathbf{C} = \mathbf{I}$) were added to fully turbulent Newtonian flows. In regions dominated by elongational strains, the response leads to a significant increase of the local viscosity, which causes a transient drag increase and also chokes turbulent fluctuations. The flow eventually relaxes to a drag reduced flow. Such initial conditions were used in some simulations discussed here.

To test our hypothesis, we also propose to perform DNS of transition to turbulence in a periodic channel flow. Compared with a spatially developing simulation, the periodicity transforms the evolution of the transition from space to time. The Reynolds number, based on the half height, h, of the domain and the bulk velocity, U_b, is identical to Dubief *et al.* (2004), $Re_b = 5,000$. Several simulations were performed to identify the scales at play during the transition process, and a domain of dimensions $6h \times 2h \times 3h$ and resolution $256 \times 128 \times 128$ captures adequately the mechanisms of transition in a polymeric flow. Using viscous scales from fully developed Newtonian turbulence, the dimensions in wall units are $1,800 \times 600 \times 900$.

Forced isotropic turbulence with and without polymers is first simulated in a periodic domain with same dimensions as the channel. A fully develop flow field is then interpolated on the grid of the channel at time $t = 0$, thus simulating the entrance region of a channel with growing boundary layers. The initial level of turbulence is weak, of the order of 1 to 2% of the bulk velocity. The turbulence in the core of the channel allows for bypass transition in Newtonian flows. For polymeric flows, polymers stretch almost to full extent in the growing boundary layers owing to the large shear in these regions. Compared with an initial condition based on instabilities derived from linear theory, this method does not force the user to presume the effects of polymers on such instabilities.

3.2.1. *Drag reduction*

Several simulations were performed at much larger We and polymer length L than previously published. Using fully developed turbulence as boundary conditions, drag reduction was explored for $L = 100$ over $We_\tau \in [120; 320]$, where $We_\tau = \lambda u_\tau^2/\nu$. Transition to turbulence in polymeric flows were run for $L = 160$ and $We_\tau = 320$ and 720 to the influence of We_τ on drag reduction. An additional simulation was performed for $L = 160$ and $We_\tau = 320$ using fully developed turbulent initial conditions. As shown in Fig. 2a, all simulations achieved drag reduction larger than 68.3%. The longest polymers $L = 160$ produced lower drag reduction than $L = 100$ and high We_τ caused a small reduction of DR. Simulations at higher We_τ for $L = 100$ are still running at the time of the sub-

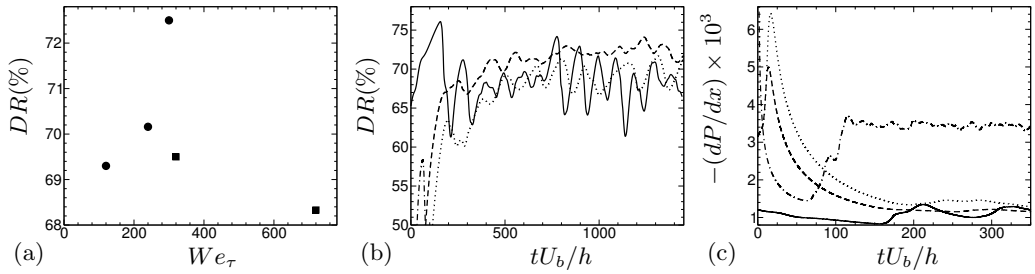

FIGURE 2. Drag reduction of several simulations approaching MDR as a function of We_τ (a): • , $L = 100$; ■ , $L = 160$. (b) and (c) Show the evolution drag reduction and pressure gradients of one transitional polymeric flow simulation (——— , $L = 160, We_\tau = 720$, 2% initial turbulent intensity) and two polymeric flow simulations started from fully developed turbulence: – – – – ($L = 100, We_\tau = 320$); ····· ($L = 160, We_\tau = 320$). A transitional Newtonian flow (—·— , 5% of initial turbulent intensity) is added as a reference.

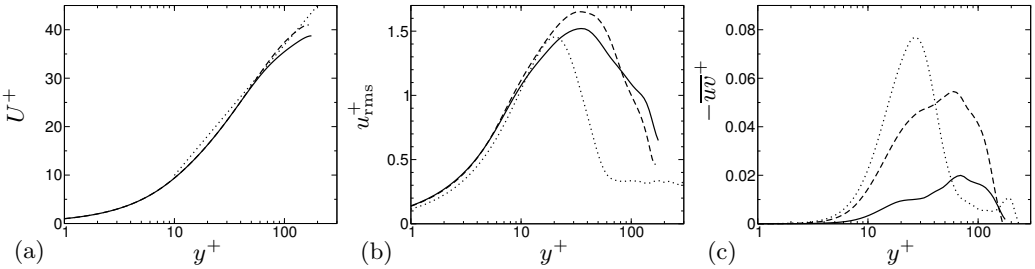

FIGURE 3. Mean velocity U^+, rms of streamwise velocity fluctuations $u^+_{\rm rms}$ and Reynolds shear $-\overline{uv}^+$ in the MDR steady state resulting from: ∘ , DNS of transition in polymeric flow ($L = 160, We_\tau = 720$); □, DNS initiated from fully developed turbulence ($L = 100, We_\tau = 320$). For reference, the data of Wu & Moin (2009) is plotted for $Re_\theta = 200$ (——— , pre breakdown) and $Re_\theta = 300$ (– – – – , post breakdown). Virk's asymptotic velocity profile (Eq. 1.1) is shown as ▬▬ .

mission of the present brief. By construction of the constitutive model, the Weissenberg number, L and β are interrelated. Thus the present study would be equivalent to an experimental study based on different polymers species and concentration, by opposition to classical experiments that only increase concentration. The merit of our approach is to identify an adverse effect of L on drag reduction. A similar and more dramatic, non-monotical behavior was observed in heat transfer (Dubief 2010*b*). The difference between the highest drag reduction at $L = 100$ and $L = 160$ is observed in Fig. 2b with much higher fluctuations of the DR at the highest polymer length. This suggests that MDR for $L = 160$ oscillates between two states, with the upper DR state being very close to the highest drag reduction simulated for $L = 100$.

Lastly, Fig. 2c displays the transient behavior of the pressure gradient from the two different initial conditions. Note that the significant drag overshoot is caused by the increase of elongational viscosity as discussed above. The simulation of transition to turbulence was unintentionally performed with a weak initial turbulent intensity (1%) that caused the Newtonian flow to become laminar. Interestingly, the polymeric flow, using the same initial condition, achieved transition.

3.3. *Velocity statistics*

Figure 3 mirrors Fig. 1 with the highest drag reduction state ($L = 100; We_\tau = 320$) available and the most fluctuating state ($L = 160; We_\tau = 720$). Both simulations follow Virk's velocity profile closely, with only a small departure for the longer polymer simulation (Fig. 3a). The streamwise velocity fluctuations (Fig. 3b) are comparable in magnitude to pre-breakdown state ($Re_\theta = 200$) of Wu & Moin (2009) DNS; however, the position of the peak is shifted upward by a little over 10 wall units. The Reynolds shear stress, shown in Fig. 3c, is much more sensitive to the polymer characteristics, as its value for $L = 100$ is twice that for $L = 160$, which indicates a larger contribution of the polymer stress, τ_{xy}, to the stress budget of the flow (Dubief *et al.* 2004, 2005). The shape of the Reynolds shear stress distribution is very different from the pre-breakdown Newtonian state, with two additional inflection points around the maximum of $-\overline{uv}^+$. In conclusion, although the mean velocity is similar to the Newtonian transitional state of breakdown of linear instabilities, the turbulent structures are significantly affected by the presence of polymers and thus differ from Newtonian flow.

4. Flow structure and the role of purely elastic instabilities

The startling discovery of this work is the onset of MDR in our viscoelastic simulation, with $L = 160$ and $We_\tau = 720$ from initial conditions that fail to cause transition in the Newtonian flow at the same Reynolds number. Figure 4 displays the evolution of the viscoelastic transition to turbulence through four snapshots chosen for their relevance. After a short quiescent state, three pairs of streaks emerge (Fig. 4a), followed quickly by a streamwise instability. The streamwise and spanwise wavelengths initially match the wavelengths of periodicity of our initial conditions (not shown). Before the onset of breakdown (Fig. 4a), the wavelength of the streamwise instability becomes much smaller. The streaks eventually break down to create two large hairpin vortices identified by positive regions of the second invariant, Q, of the velocity gradient $\boldsymbol{\nabla}\mathbf{u}$. As pointed out by Dubief & Delcayre (2000), the isosurfaces of positive Q isolate regions where the local rotation rate overcomes the local strain rate, which also correlate to region of local minima of pressure since $Q = \nabla^2 p$. Using a low threshold, Fig. 4b shows two types of structures at the breakdown: large scale vortices and smaller scales. The former category includes two hairpin vortices and their satellite vortices. The latter consists of trains of thin rolls found in the wake of the large scale vortices, as shown in Figs. 4b and 4c. These structures appear to be pressure minima only, not vortices. Following on the discussion of the drag fluctuations (Fig. 2), this MDR regime fluctuates between a quiescent regime, as depicted by Fig. 4c, where even a threshold of Q as low as 0.1 cannot educe vortices, to the breakdown regime shown in Fig. 4c. These two regimes correspond to the minima and extrema of drag shown in Fig. 2. The quiescent state is characterized by significant polymer activity in the outer region of the flow as observed in Fig. 4c, which is reminiscent of a breakdown state. During a breakdown event(Figs 4b,d), polymers in the core of the flow show less activity. This observation illustrates the phase shift that exists between growth of vortices and the polymer dynamics needed to constraint the vortices' growth. It is that interplay of time scales that should ultimately be a critical factor in the level of drag reduction a particular polymer solution may achieve.

The cause for the onset of turbulence and the generation of the small scales observed with positive isosurfaces of Q is found in purely elastic instabilities of polymeric flows. The review of Shaqfeh (1996) describes several instabilities entirely driven by polymer

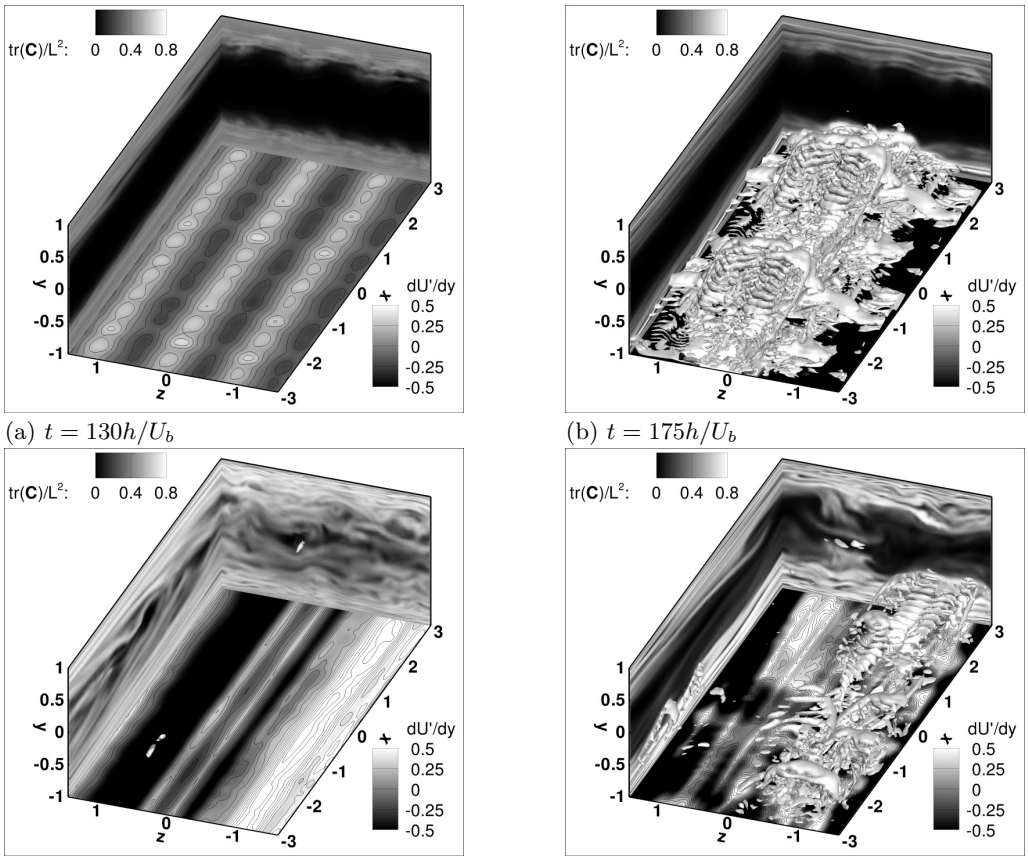

(a) $t = 130h/U_b$ (b) $t = 175h/U_b$

(c) $t = 230h/U_b$ (d) $t = 1040h/U_b$

FIGURE 4. Flow visualizations at different times in the transition of a polymeric channel flow to MDR. Regions of positive second invariant of velocity tensor are shown as white isosurfaces for $Q = 0.1$. The lower wall displays contours of fluctuation of wall shear. Only the lower half of the domain is shown for clarity.

dynamics that occur in low-inertia flows. An instability similar to the type observed in Taylor-Couette flow has recently been observed in Rayleigh-Benard flows by Dubief (2010*a*,*b*). In the former, two-dimensional simulations of natural convection demonstrate the existence of trains of local pressure minima (and maxima) in convection plumes, where polymers are significantly elongated. Figure 5 isolates one of the trains of local pressure minima, shown by isosurfaces of $Q = 0.1$. In the train of pressure minima isolated in Fig. 5a, each region of pressure local minima or maxima extends over 3 to 5 computational nodes in all directions. Further refinement (not shown) of the grid have also confirmed that this interesting pattern is not the result of a numerical instability. Similar to convection plumes, these minima are found in region of large polymer elongation, in this case caused by the head of an hairpin vortex, which causes the large region of polymer stretch underneath the streamlines (Fig. 5b). Figure 5a focuses on the flow streamlines computed from the fluctuating velocity vector field. The waviness of these streamlines is correlated to local minima and maxima of pressure. In the frame of reference of the flow being extended upward in the wake of the head of hairpin vortex,

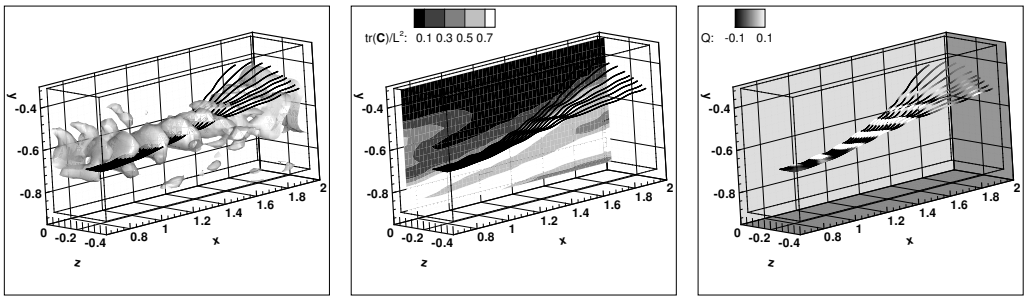

(a) Isosurfaces of $Q = 0.1$ (b) Polymer elongation (c) Streamlines colored by Q

FIGURE 5. Study of a train of small scales produced in the wake of vortex observed in Fig. 4d. The streamlines are computed from the velocity fluctuations to highlight the small deformations caused by the successive local minima of pressure on the velocity field. Polymer elongation and isosurfaces are shown to correlate the spatial location of the train to an extended region of large polymer elongation.

local minima induce an upward deformation of the streamlines whereas local maxima create downward deformation. The detailed study of the mechanism of viscoelastic transition could not be completed in time, but analysis of animations (not shown) suggests that similar elastic instabilities are created in the wall-streaks during the transition (see Fig. 4a), causing the streaks to eventually breakdown and form vortices.

The discovery of the existence of purely elastic instability in transitional flow and MDR was made possible by the combination of a robust numerical method and a very fine resolution in the streamwise direction. In Dubief *et al.* (2005), we demonstrated that our treatment of the advection term, directly derived from Min *et al.* (2001), captures the essence of the small scale dynamics of the configuration tensor transport equation (Eq. 3.4). Using Batchelor's theory (Batchelor *et al.* 1959) for the transport of low-diffusion passive scalars ($Sc \gg 1$, Schmidt number is the ratio of solvent viscosity to scalar diffusivity), we used the typical time-scale of each term in Eq. (3.4) to argue that the spectral behavior of the fluctuations of polymer stress should essentially follow the k^{-1} behavior of passive scalars at high wavenumbers. Such a behavior was indeed obtained by the combination of upwind compact schemes and local artificial dissipation, whereas the application of a global dissipation term to Eq. (3.4) was found to dramatically attenuate the small scale dynamics of polymer stress. The critical role that these instabilities seem to have in the transition to turbulence of polymeric wall flows and the fluctuations of subsequent MDR states supports our 2005 discussion and the need for numerical methods that can accurately capture the small scale dynamics of polymers in solution.

5. Conclusion

The research conducted during the CTR summer program yielded three major advances in the understanding of polymer drag reduction:(a) the first simulations of MDR in domains larger than minimal flow units; (b) the identification of purely elastic instabilities and their role in the onset of MDR in viscoelastic transitional flows as well as their impact on the flow dynamics at MDR; (c) the definition of MDR as a unique transitional state: the breakdown of linear instabilities. Item (c) presents a critical step toward the prediction of MDR as a function of polymer parameters and boundary conditions. It is important to remember that the present definition is based on Virk's log law,

which appears to be a universal feature of transitional flows in Newtonian and polymeric fluids, and independent of initial conditions (as our on-going study of transition to turbulence with different initial conditions seems to suggest). The identification of MDR as a unique transitional state does not predict quantitatively the magnitude of drag reduction, only the flow topology. However, our definition narrows the field of investigation to the fundamentals of transition in wall-bounded flows and the interactions between flow instabilities, polymer stress and elastic instabilities.

Acknowledgments

YD gratefully acknowledges computational support from the Vermont Advanced Computing Center, and P. Moin and CTR for their invitation to the 2010 summer program. The authors thank Prof. Xiaohua Wu for sharing his database of transitional boundary layer flow.

REFERENCES

Batchelor, G. K., Howells, I. D. & Townsend, A. A. 1959 Small-scale variation of convected quantities like temperature in turbulent fluid part 2. the case of large conductivity. *J. Fluid Mech.* **5** (01), 134–139.

Bird, R., Armstrong, R. & Hassager, O. 1987 *Dynamics of Polymeric Liquids. Vol. 2: Kinetic Theory*. Wiley-Interscience, 1987,.

De Angelis, E., Casciola, C. & Piva, R. 2002 DNS of wall turbulence: dilute polymers and self-sustaining mechanisms. *Computers & Fluids* **31** (4-7), 495–507.

Dimitropoulos, C., Dubief, Y., Shaqfeh, E. & Moin, P. 2006 Direct numerical simulation of polymer-induced drag reduction in turbulent boundary layer flow of inhomogeneous polymer solutions. *J. Fluid Mech.* **566**, 153–162.

Dimitropoulos, C., Dubief, Y., Shaqfeh, E., Moin, P. & Lele, S. 2005 Direct numerical simulation of polymer-induced drag reduction in turbulent boundary layer flow. *Phys. Fluids* **17**, 011705.

Dubief, Y. 2010*a* Elastic instabilities in two-dimensional natural convection. *In preparation* .

Dubief, Y. 2010*b* Heat transfer enhancement and reduction by poylmer additives in turbulent Rayleigh Benard convection. *Arxiv preprint arXiv:1009.0493* Submitted to *Phys. Rev. Lett.*

Dubief, Y. & Delcayre, F. 2000 On coherent-vortex identification in turbulence. *J. of Turbulence* **1** (011).

Dubief, Y., Terrapon, V., White, C., Shaqfeh, E., Moin, P. & Lele, S. 2005 New answers on the interaction between polymers and vortices in turbulent flows. *Flow, turbulence and combustion* **74** (4), 311–329.

Dubief, Y., White, C., Terrapon, V., Shaqfeh, E., Moin, P. & Lele, S. 2004 On the coherent drag-reducing and turbulence-enhancing behaviour of polymers in wall flows. *J. Fluid Mech.* **514**, 271–280.

Jimenéz, J. & Moin, P. 1991 The minimal flow unit in near-wall turbulence. *J. Fluid Mech.* **225**, 213–240.

Kim, K., Li, C., Sureshkumar, R., Balachandar, S. & Adrian, R. 2007 Effects of polymer stresses on eddy structures in drag-reduced turbulent channel flow. *J. Fluid Mech.* **584**, 281–299.

Min, T., Choi, H. & Yoo, J. 2003 Maximum drag reduction in a turbulent channel flow by polymer additives. *J. Fluid Mech.* **492**, 91–100.

Min, T., Yoo, J. & Choi, H. 2001 Effect of spatial discretization schemes on numerical solutions of viscoelastic fluid flows. *J. Non-Newtonian Fluid Mech.* **100** (1-3), 27–47.

Ptasinski, P., Boersma, B., Nieuwstadt, F., Hulsen, M., Van Den Brule, B. & Hunt, J. 2003 Turbulent channel flow near maximum drag reduction: simulations, experiments and mechanisms. *J. Fluid Mech.* **490**, 251–291.

Shaqfeh, E. 1996 Purely elastic instabilities in viscometric flows. *Ann. Rev. Fluid Mech.* **28**, 129–185.

Somandepalli, V., Hou, Y. & Mungal, M. 2010 Concentration flux measurements in a polymer drag-reduced turbulent boundary layer. *J. Fluid Mech.* **644**, 281–319.

Sureshkumar, R., Beris, A. & Handler, R. 1997 Direct numerical simulation of the turbulent channel flow of a polymer solution. *Phys. Fluids* **9**, 743.

Virk, P., Mickley, H. & Smith, K. 1970 The ultimate asymptote and mean flow structure in Toms phenomenon. *Trans. ASME E: J. Appl. Mech* **37**, 488–493.

Warholic, M., Massah, H. & Hanratty, T. 1999 Influence of drag-reducing polymers on turbulence: effects of Reynolds number concentration and mixing. *Exp. fluids* **27** (5), 461–472.

White, C., Somandepalli, V. & Mungal, M. 2004 The turbulence structure of drag-reduced boundary layer flow. *Exp. Fluids* **36** (1), 62–69.

Wu, X. & Moin, P. 2009 Direct numerical simulation of turbulence in a nominally zero-pressure-gradient flat-plate boundary layer. *J. Fluid Mech.* **630**, 5–41.